

Magnetism and Electronic Correlations in Quasi-One-Dimensional Compounds

M. D. Coutinho-Filho,*^a R. R. Montenegro-Filho,^a E. P. Raposo,^a C. Vitoriano^b and M. H. Oliveira^c

^aLaboratório de Física Teórica e Computacional, Departamento de Física, Universidade Federal de Pernambuco, 50670-901 Recife-PE, Brazil

^bUniversidade Federal Rural de Pernambuco, Unidade Acadêmica de Garanhuns, 55296-190 Garanhuns - PE, Brazil

^cUniversidade Federal Rural de Pernambuco, Unidade Acadêmica de Serra Talhada, 56900-000 Serra Talhada - PE, Brazil

Nesta contribuição à celebração do octogésimo aniversário de nascimento do Prof. Ricardo Ferreira, apresentamos uma breve discussão sobre compostos magnéticos quase-unidimensionais. Esta tem sido uma área de pesquisa de intensa atividade, particularmente após a divulgação de verificações experimentais de magnetismo em polímeros organometálicos na década de 1980. Neste trabalho realizamos uma revisão das contribuições teóricas e experimentais sobre o assunto, com foco em sistemas de elétrons correlacionados em cadeias com célula unitária do tipo AB_2 presentes em compostos inorgânicos e orgânicos.

In this contribution on the celebration of the 80th birthday anniversary of Prof. Ricardo Ferreira, we present a brief survey on the magnetism of quasi-one-dimensional compounds. This has been a research area of intense activity particularly since the first experimental announcements of magnetism in organic and organometallic polymers in the mid 80's. We review experimental and theoretical achievements on the field, featuring chain systems of correlated electrons in a special AB_2 unit cell structure present in inorganic and organic compounds.

Keywords: quasi-one-dimensional systems, ferrimagnetism, Hubbard model, Heisenberg model

1. Introduction

The magnetism of organic¹⁻³ and organometallic⁴ polymers has been a challenging topical field since its first experimental announcements. This rapidly growing and interdisciplinary research area also includes inorganic compounds,⁵ with ferro- and ferrimagnetic long-range order (see Section below). In this work we briefly review some attempts to describe the ground state and the low-temperature thermodynamics of these compounds. In particular, we report on analytical and numerical results on polymeric chains of correlated electrons in special unit cell topologies shown in Figure 1.

2. Quasi-One-Dimensional Magnetic Compounds: A Brief Review

Despite many years of experimental and theoretical efforts, the complete understanding and precise

characterization of magnetism and electronic correlations in quasi-one-dimensional (quasi-1d) compounds still offer great scientific challenges and technical difficulties.³ Regarding, for instance, organic magnetic polymers, it is known³ that their magnetic properties are ascribed to the correlated p-electrons of light elements, such as C, O, and N, in contrast to the magnetism found in transition and rare-earth metals due to partially filled d or f orbitals. For this reason it took many years of efforts on the synthesis and characterization of a great variety of compounds before the announcement of bulk ferromagnetism (FM) in an organic polymer.¹ In Figure 1(b) we sketch this material made of polyacetylene-based radicals, R^* , containing unpaired residual electrons, i.e. *poly*-BIPO or poly[1,4-bis(2,2,6,6-tetramethyl-4-piperidyl-1-oxyl)-butadiyne]. However, this compound presented several problems due to its insolubility and poor reproducibility both in the preparation and in the magnetic results.³ Later, Nishide and collaborators⁶ have successfully synthesized polyphenylacetylenes with various types of radical groups. These polymers exhibit similar band structure schemes⁷ comprising filled bonding

*e-mail: mdcf@ufpe.br

molecular-orbital bands, empty antibonding bands, and narrow half-filled nonbonding bands, usually just one at the center of the band. A net magnetic moment may appear either because the number of itinerant antiferromagnetically (AF)-correlated σ electrons per unit cell is odd and/or due to the presence of localized electrons.^{1,7}

A seminal work has also been performed by Takahashi and collaborators in order to extensively characterize the long-range macroscopic FM behavior found in the organic compound *p*-nitrophenyl nitroxyl nitroxide radical (*p*-NPNN, in the ι and δ phases).^{2,8} Actually, the excellent fitting of the low-temperature (T) experimental data is consistent with predictions from the thermodynamic Bethe-ansatz solution of the 1d-quantum FM Heisenberg model:⁸ susceptibility $\epsilon \sim T^{-2}$ and specific heat $C \sim T^{1/2}$ as $T \rightarrow 0$.

Other organic magnets have been synthesized, such as polyradicals derived from poly(1,3-phenylenemethylene) and polyphenylenevinylene-based radicals.³ In these cases the polymer structure is made of benzene rings linked by divalent carbon atoms or including pendant radicals with oxygen atoms carrying an uncompensated electron.³ Another family of organic magnetic polymers is that of the doped poly(*m*-aniline) compounds, in which the carbon atoms responsible for the links between the benzene rings are substituted by ionized nitrogen with a H-bond or a radical plus a charge acceptor.⁹ On the other hand, doped polypyrrole compounds also exhibit¹⁰ interesting magnetic properties and Drude metallic response as well.

A distinct class of magnetic polymers combines metal ions with organic complexes, displaying a rich variety of magnetic behaviors, such as ferro- and ferrimagnetism, AF and canted AF and spin glass phase.^{11,12} In fact, the first experimental observation of a magnet with spin residing in a p-orbital was performed in the compound $[\text{Fe}(\text{C}_5\text{Me}_5)_2]^+[\text{TCNE}]^-$ (TCNE = tetracyanoethylene).⁴ Some homometallic ferrimagnets with chain structure^{13,14} involve the compounds^{15,16} $M_2(\text{EDTA})(\text{H}_2\text{O})_4 \cdot 2\text{H}_2\text{O}$ ($M = \text{Ni}, \text{Co}$; EDTA = ethylenedi-amine tetraacetate = $\text{C}_{10}\text{N}_2\text{O}_8$) and $M(\text{R-py})_2(\text{N}_3)_2$ ($M = \text{Cu}, \text{Mn}$; R-py = pyridinic ligand = $\text{C}_5\text{H}_4\text{N-R}$ with $R = \text{Cl}, \text{CH}_3$, etc.).¹⁷⁻²⁰ Regarding bimetallic chain materials, the compound²¹ $\text{MnCu}(\text{pbaOH})(\text{H}_2\text{O})_3$ [pbaOH = 2-hydroxy-1, 3-propylenebis(oxamato) = $\text{C}_7\text{H}_6\text{N}_2\text{O}_7$] has been one of the first synthesized which retains long-range FM or ferrimagnetic order on the scale of the crystal lattice, as in the case of isomorphous realizations.²²⁻²⁴ Heterometallic chain structures have also been object of systematic study.^{25,26} More recently, the metal-radical hybrid strategy, combined with fabrication of novel polyradicals,²⁷ has led to the synthesis of a variety of heterospin chain compounds.^{28,29} Several of these

compounds display 1d ferrimagnetic behavior^{30,31} modeled by alternating spin chains³² such as, for instance, those with the structure shown in Figure 1(c).

Of recently growing interest we mention the quasi-1d chains with AB_2 and $ABB\infty$ unit cell structure [henceforth referred to as AB_2 chains; see Figures 1(a) and (b)]. Such structures are found both in inorganic and organic ferrimagnetic compounds. Regarding inorganic materials, we cite the homometallic compounds with a line of trimer clusters characteristic of phosphates of formula $A_3\text{Cu}_3(\text{PO}_4)_4$, where $A = \text{Ca}$,³³⁻³⁶ Sr ,³⁴⁻³⁷ and Pb .^{35,36,38} The trimers have three Cu^{+2} paramagnetic ions of spin $S = 1/2$ AF coupled. Although the superexchange interaction is much weaker than the intratrimer coupling, it proves sufficient to turn them into bulk ferrimagnets. Furthermore, compounds of formula $\text{Ca}_{3-x}\text{Sr}_x\text{Cu}_3(\text{PO}_4)_4$, $0 \leq x \leq 3$,³⁷ hybrid analogous to the mentioned phosphates, have also been synthesized in an attempt to tune the AF bridges between Cu sites and possibly explore how paramagnetic spins grow into bulk ferrimagnets. It is also interesting to mention the frustrated AB_2 inorganic compound³⁹ $\text{Cu}_3(\text{CO}_3)_2(\text{OH})_2$, which displays low- T short-range magnetic order and has its physical properties well described through the distorted diamond chain model.⁴⁰ At last, we observe that the AB_2 structure is also present⁴¹ in the organic ferrimagnetic compound 2-[3',5'-bis(*N*-*tert*-butylaminoxyl)phenyl]-4,4,5,5-tetramethyl-4,5-dihydro-1H-imidazol-1-oxyl 3-oxide, or PNNBNO, consisting of three $S = 1/2$ paramagnetic radicals in its unit cell.

3. Magnetic Chains with AB_2 Unit Cell Topology: Analytical and Numerical Studies

In this section we model and discuss analytical and numerical results on the magnetic chains with AB_2 and $ABB\infty$ unit cell topologies displayed in Figures 1(a) and (b). Eventually, alternate spin chains shown in Figure 1(c) are also considered. A rigorous theorem by Lieb⁴² predicts that bipartite AB_2 chains modeled through a Hubbard Hamiltonian [see equation (1) below], with one electron per site on average (half-filled limit) and repulsive Coulombian interaction, present average ground-state spin per unit cell $\hbar/2$ and quantum ferrimagnetic long-range order at $T = 0$.⁴²⁻⁴⁵ The magnetic excitations on this state have been studied in detail both in the weak- and strong-coupling limits,⁴⁶ and in the light of the quantum AB_2 Heisenberg model.⁴⁶⁻⁴⁸ Further studies have considered the anisotropic⁴⁹ and isotropic⁵⁰ critical behavior of the quantum AB_2 Heisenberg model, including its spherical version,⁵¹ and the statistical mechanics of the classical AB_2 Heisenberg model.⁴⁸

Away from half-filling, doped AB_2 Hubbard chains were previously studied through Hartree-Fock, exact diagonalization and quantum Monte Carlo techniques both in the weak- and strong-coupling limits,^{43,52} including also the $t - J$ model,⁵³ using the density-matrix renormalization group and recurrent variational *Ansätze*s, and the infinite Coulombian repulsion limit⁵⁴ using exact diagonalization. In particular, these chains represent an alternative route to reaching $2d$ quantum physics from $1d$ systems.^{53,55}

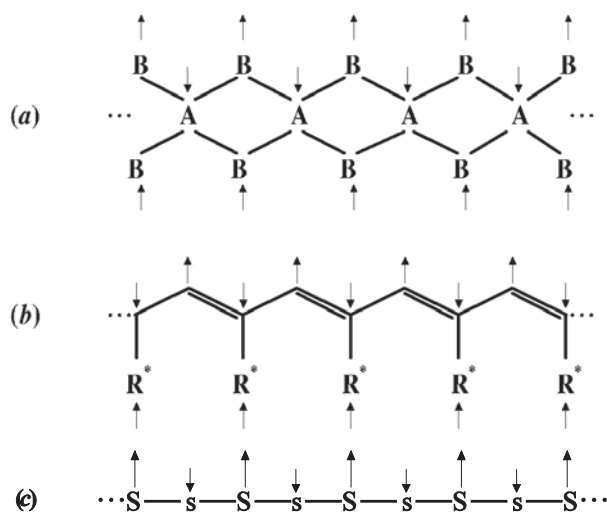


Figure 1. Ferrimagnetic ground-state configurations of (a) bipartite lozenge AB_2 chains, (b) substituted polyacetylene, with lateral radicals R^* as B sites containing unpaired residual electrons, and (c) alternate spin chains.

3.1 Analytical results

We start considering the AB_2 chain modelled through the one-band Hubbard model, which is the simplest lattice model for strongly correlated materials:

$$H = -t \sum_{\langle i\alpha, j\beta \rangle, \sigma} c_{i\alpha, \sigma}^+ c_{j\beta, \sigma} + U \sum_{i\alpha} n_{i\alpha \uparrow} n_{i\alpha \downarrow} \quad (1)$$

where $c_{i\gamma, \phi}^+$ ($c_{i\gamma, \phi}$) is the creation (annihilation) operator for electrons with spin ϕ ($= \uparrow, \downarrow$) at site $\gamma = A, B_1$ or B_2 of the unit cell i , t is the hopping parameter, U is the intrasite Coulomb repulsion and, in the first summation, $i\gamma$ and $j\delta$ are nearest neighbor sites. We define N as the total number of sites and N_c ($= N/3$) as the number of unit cells. We remark that in the limit $U = \infty$ the Hubbard Hamiltonian reduces to a hopping term with double site occupancy excluded.⁵²

In the tight-binding description ($U = 0$), this model presents three bands: one flat with N_c localized orbitals with energy $\eta = 0$, and two dispersive with $\eta_{\pm} = \pm 2t \cos(q/2)$, where $q = 2\sigma/N_c$ and $l = 0, \dots, N_c - 1$. At half-filling ($N_e = N$, where N_e is the number of electrons) and $U = 0$ the ground

state (GS) total spin quantum number S_g is degenerate, with S_g ranging from the minimum value (0 or 1/2) to $S_g = |N_B - N_A|/2 = N_c/2$, where N_A (N_B) is the number of sites in the A (B) sublattice. As proved by Lieb⁴² in the general case of any bipartite lattice with $N_B \in N_A$, the Coulomb repulsion lifts this huge degeneracy and selects the state with $S_g = |N_B - N_A|/2$ to be the unique GS of the system, apart from the trivial $(2S_g + 1)$ -fold rotational degeneracy.

In the strong coupling limit ($U \gg t$) and at half-filling the AB_2 Hubbard Hamiltonian, equation (1), is mapped^{50,56} onto the quantum $S = 1/2$ Heisenberg model with $O(n)$, $n = 3$, rotational symmetry:

$$H = \sum_{ij} \sum_{\alpha\beta} J_{ij}^{\alpha\beta} \mathbf{S}_{i\alpha} \cdot \mathbf{S}_{j\beta} \quad (2)$$

where the localized spins $\mathbf{S}_{i\gamma}$ interact antiferromagnetically through $J_{ij}^{\delta} = J = 4t^2/U > 0$. In fact, Lieb and Mattis have shown⁵⁷ that the Heisenberg model in a bipartite lattice has also $S_g = |N_B - N_A|/2$, which indicates that $S_g = N_c/2$ for the AB_2 Heisenberg model, as in the Hubbard case. Eventually, in the presence of an uniform magnetic field \mathbf{H} along the z direction, a Zeeman energy term, $-(g\mu_B H/\hbar) \sum_{i\gamma} S_{z_{i\gamma}}$, is added to equation (2), where g is the gyromagnetic factor and μ_B is the Bohr magneton (in what follows we take units in which $g\mu_B \neq 1$). In $H = 0$ the ground-state of the system exhibits^{42,43} unsaturated FM or ferrimagnetic configurations as indicated in Figures 1(a) and (b), with average spin per unit cell $\langle S_{cell}^z \rangle = \hbar/2$ (Lieb's theorem⁴²). In addition, we can also model the alternate spin chains shown in Figure 1(c) by considering in equation (2) $\mathbf{S}_{i\gamma} = \mathbf{S}_i$ and $\mathbf{S}_{i\delta} = \mathbf{s}_i$, with $S > s$. Such model systems have been used to describe^{31,32} a number of organometallic compounds in which, e.g., $S = 5/2$ or $S = 2$ and $s = 1/2$.

The Euclidean action of the partition function in a coherent-state \mathbf{n} -field representation,⁵⁸ $T = \int D\mathbf{n} \exp(-S_E/\hbar)$, is given by $S_E = S_{exc} + S_{WZ} + S_Z$, with contributions from exchange and Zeeman interactions, and a topological Wess-Zumino term, which is a Berry's phase-like term associated with the time evolution of the spin due to quantum fluctuations.⁵⁸ The low-lying properties of the quantum ferrimagnetic chains in Figure 1 are dominated by infrared fluctuations around the Néel configuration. In order to obtain their effective low-lying action, we take staggered dimensionless unit coherent magnetization fields and split the topological term in a FM and an AF contribution, $S_{WZ} = S_{WZ}^{AF} + S_{WZ}^{FM}$ following the spin structure of the polymer. Then, taking the continuum limit and integrating out the rapidly fluctuating field modes, we obtain the low-energy effective action, $S_{eff} = \int_0^L dx/(2a) \int_0^{\beta\hbar} d\tau E$, where L is the length of the chain of lattice parameter $2a$, and $\beta \notin (k_B T)^{-1} = i/\hbar$ expresses the result of a Wick

rotation to imaginary times it . The Lagrangian density is $E = E_{\phi NL} + E_{WZ}^{FM} + E_Z + E_{irrel}$ where

$$\Lambda_{\sigma NL} = \Lambda_{exc} + \Lambda_{WZ-exc}^{AF} = \alpha_x (\partial_x \mathbf{m})^2 + \alpha_\tau (\partial_\tau \mathbf{m})^2 \quad (3)$$

corresponds to the quantum nonlinear (NL) ϕ model, with unit magnetization fields $\mathbf{m}^2 = 1$,

$$\Lambda_{WZ}^{FM} = -i \sum \hbar \int_0^1 d\gamma \partial_\gamma \mathbf{m} \cdot (\mathbf{m} \times \partial_\tau \mathbf{m}) \quad (4)$$

represents the contribution from the FM Wess-Zumino term, and E_{irrel} are irrelevant terms in the renormalization group (RG) context. In equations (3) and (4), $\gamma_x = 2JS^2\hbar^2 a^2$, $\gamma_\chi = 1/(8J)$, and $M = S$ for the AB_2 chains, whereas $\gamma_x = JS^2\hbar^2 a^2$, $\gamma_\chi = s/(4JS)$, and $M = S - s$ for the alternate spin chains of Figure 1. The FM Wess-Zumino term is responsible for the ferrimagnetic ground states. Indeed, $E_{WZ}^{FM} = 0$ in either cases of AB or $S = s$ chains. Those represent usual quantum AF Heisenberg chains, which are known to follow Haldane's conjecture,⁵⁹ i.e. half-integer spin chains are critical with no long-range order and integer spin chains are disordered. Moreover, the addition of the relevant Wess-Zumino term to the quantum NL ϕ model, equation (3), changes its properties dramatically since the critical dynamical exponent assumes $z = 2$ (nonrelativistic feature), in contrast with the value $z = 1$ found in the relativistic quantum NL ϕ model, associated with the $2d$ -quantum AF Heisenberg Hamiltonian. In fact, equation (4) corresponds to the field-theoretical version of the topological constraints imposed by the polymer structure, as identified by semi-empirical methods.^{1,60,61}

We now perform a momentum-shell low- T RG study of the system (see references 62 and 63 for similar treatments of the classical and quantum $z = 1$ NL ϕ models). First, we decompose the magnetization fields into transversal and longitudinal components, integrate over the latter one, expand the resulting action, $S_{eff} = S^{(2)} + S^{(4)} + \dots$, and Fourier transform the terms to the momentum- k and Matsubara frequency- ϑ_n space, with $\vartheta_n = 2\sigma n/u$, $n = 0, \pm 1, \pm 2, \dots$, $u = \overline{\omega}$, and $\overline{\omega} = \sigma^2 JS\hbar^2$ or $\overline{\omega} = \sigma^2 JSs\hbar^2/(S - s)$ respectively for the AB_2 or alternate spin chains. The quadratic term in the diagonal field space $\{\theta^*, \theta\}$ reads⁵⁰

$$\frac{S^{(2)}(\mathbf{k}, \omega_n)}{\hbar} = \sum_{n=-\infty}^{+\infty} \int_{BZ} \frac{d^d k}{(2\pi)^d} \frac{u}{g_0} (k^2 - i\omega_n + hg_0) + \frac{\lambda_d \pi^2}{2} \omega_n^2 - \frac{\rho g_0}{u} \phi^*(\mathbf{k}, \omega_n) \phi(\mathbf{k}, \omega_n) \quad (5)$$

where $hg_0 \notin H\overline{\omega}\hbar$, the density of degrees of freedom ν comes from the integration over the longitudinal components, and the meaning of ν_d is discussed below. The bare coupling

is defined as $g_0 \notin \sigma/\text{Min } d = 1$. The quartic contribution is given by⁵⁰

$$\frac{S^{(4)}(\mathbf{k}, \omega_n)}{\hbar} = \sum_{n_1, \dots, n_4 = -\infty}^{+\infty} \int_{BZ} \left[\prod_{i=1}^4 \frac{d^d k_i}{(2\pi)^d} \right] \frac{u}{g_0} \left[\frac{1}{2} (-\mathbf{k}_2 \cdot \mathbf{k}_4 + \mathbf{k}_2 \cdot \mathbf{k}_3 + \mathbf{k}_1 \cdot \mathbf{k}_4 - \mathbf{k}_1 \cdot \mathbf{k}_3) + \frac{i\pi \hbar g_0}{\sqrt{2}} \sum_{j=1}^d (k_{j,4} - k_{j,3}) \right. \\ \left. + \frac{\hbar g_0}{2} - \frac{i}{4} (\omega_{n_3} + \omega_{n_4}) - \frac{\pi}{\sqrt{2}} \sum_{j=1}^d (\omega_{n_3} k_{j,4} - \omega_{n_4} k_{j,3}) \right. \\ \left. + \lambda_d \frac{11\pi}{96\sqrt{2}} (\omega_{n_1} \omega_{n_3} + \omega_{n_1} \omega_{n_4} + \omega_{n_2} \omega_{n_3} + \omega_{n_2} \omega_{n_4}) \right] \\ \phi^*(1)\phi(2)\phi^*(3)\phi(4)(2\pi)^d \delta(\mathbf{k}_2 + \mathbf{k}_4 - \mathbf{k}_1 - \mathbf{k}_3) \delta_{(\omega_{n_2} + \omega_{n_4}), (\omega_{n_1} + \omega_{n_3})} \quad (6)$$

In the sequence, we require that the fluctuation modes in the two-point vertex function scales homogeneously through a RG scaling transformation, $k \leftarrow bk$, $\vartheta_n \leftarrow b^z \vartheta_n$, with $b \notin e^l$. We also take the fixed point $\nu_d^* \neq 0$ for $d = 1$, as a consequence of the irrelevance of the ϑ_n^2 -dependent terms in the RG context. The one-loop equations for the renormalized coupling g , and dimensionless temperature $t \notin g/u$ and magnetic field $\overline{h} \notin hg$ in $d = 1$ and $z = 2$ read:⁵⁰

$$\frac{dg}{dl} = -(d + z - 2)g + \frac{\kappa_d}{2} g^2 \coth[g(1 + \overline{h})/2t], \\ \frac{dt}{dl} = -(d - 2)t + \frac{\kappa_d}{2} gt \coth[g(1 + \overline{h})/2t], \quad (7) \\ \frac{d\overline{h}}{dl} = 2\overline{h}, \quad \frac{du}{dl} = -zu, \quad u = \frac{g}{t}$$

We thus obtain the semiclassical fixed point: $g^* = t^* = \overline{h}^* = 0$, since $g^* = 0$ implies in $M \leftarrow \mathfrak{R}$, and the quantum critical fixed point:⁶³ $g^* \notin g_c = 2\sigma$, $t^* = \overline{h}^* = 0$. The former describes a $1d$ -classical Heisenberg ferromagnet with quantum corrections, whereas the latter is identified with a classical Heisenberg model in $d + z = 3$ dimensions. The analysis of stability shows that both fixed points are unstable under thermal fluctuations, but only the semiclassical fixed point is stable under infrared quantum fluctuations, as displayed in Figure 2.

By studying the correlation length Y and magnetic susceptibility ϵ we identify⁵⁰ three distinct quantum regimes. As $T \leftarrow 0$ and $g > g_c$, the quantum $z = 2$ NL ϕ model is in a quantum disordered phase, whereas for $g < g_c$ its ground state has long-range order, with both quantum and thermal fluctuations playing important roles. For $g = g_c$ and $T \leftarrow 0$ the system approaches the quantum critical fixed point characterized by the extinction of the spin-wave modes and the absence of long-range order. As shown in Figure 2 the quantum critical region is defined by the crossover lines $T \sim |g - g_c|^\theta$, where $\theta = z\rho_3$, with ρ_3 the

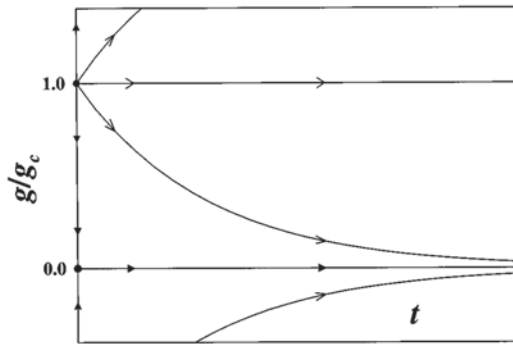


Figure 2. Schematic RG ($g, t \ni T$) flux diagram for the $1d$ -quantum $z = 2$ NL ϕ model. Semiclassical ($g^* = T^* = 0$) and quantum-critical ($g^* = g_c, T^* = 0$) fixed points are shown, as well as the flux lines indicating their stability with respect to infrared perturbations. The segment $T = 0, 0 \leq g_0 < g_c$, corresponds to the *loci* of points in which Lieb's theorem is included, with presence of stable ferrimagnetic states of quantum AB_2 and alternate spin chains.

$3d$ -Heisenberg correlation-length exponent. In particular, we find⁵⁰ the following low- T behavior in the quantum critical region:

$$\xi \sim T^{-1/z}, \chi \sim T^{-1}, C \sim T^{d/z} \quad (8)$$

with the standard result for the low- T quantum critical specific heat C and exponents satisfying scaling relations proper of this region.^{64,65} Similarly, for the $T \ll 0, g < g_c$ semiclassical region, we find

$$\xi \sim T^{-1}, \chi \sim T^{-2}, C \sim T^{1/2} \quad (9)$$

where the specific heat is determined by the spin wave contribution. In equations (8) and (9) the amplitudes of the observables cannot be completely fixed by the RG procedure. We thus identify the asymptotic low- T critical behavior described by equation (9) with that of the quantum $S = 1/2 AB_2$ and alternate spin ferrimagnetic chains, as well as that of the $1d$ -quantum $S = 1/2$ Heisenberg ferromagnet, such as the organic ferromagnetic compound p-NPNN.⁸ In addition, an interesting question arises regarding the access of such AB_2 chains in the half-filled strong-coupling limit to the quantum disordered and quantum critical regimes of the quantum $z = 2$ NL ϕ model. This scenario, if accomplished, might involve the presence of extra frustrated couplings in the unit cell structure. In any case, we would like to mention that our predicted one-loop critical behaviors for the renormalized classical and quantum critical fixed points are in agreement with those of the FM transition in $1d$ itinerant electron systems in the context of a Luttinger liquid framework.⁶⁶ However, while our localized spin disordered phase is gapped, the quantum disordered phase in reference 66 behaves as an ordinary gapless Luttinger

liquid. Obviously, further theoretical work is needed in order to clarify the physical scenario predicted for the critical behavior of the quantum NL ϕ model with a FM Wess-Zumino term due to the AB_2 topology.

In order to improve the understanding of the role of the quantum and thermal fluctuations, topology, and spin symmetry to the properties of the ferrimagnetic AB_2 chains, we have also performed a number of analytical studies using Ising, Heisenberg and spherical Hamiltonians as model systems in this unit cell structure.^{48,51,67}

First, by regarding the spin operators in equation (2) as Ising variables, $S_{i\gamma} = \pm \hbar/2$, we apply⁴⁸ the RG decimation of B sites and obtain the exact Gibbs free energy as function of the effective coupling J^* and field H^* . At zero field the ground state result $J^* = -2J < 0$ for the effective coupling between A sites indicates the presence of a ferrimagnetic structure with average spins at B sites pointing opposite to those at A sites, implying in a unit cell average spin $\langle S_{cell}^z \rangle = \hbar/2$. As H increases at $T = 0$, we notice that J^* increases linearly with H and vanishes for $H \nabla J$; conversely, H^* first decreases linearly with H for $H < J$, and then increases also linearly, changing sign at the critical field $H_c = 2J$. At $H = H_c$ a first order transition occurs with a discontinuous change of $\langle S_{cell}^z \rangle$ from $\hbar/2$ to its saturated value $3\hbar/2$ (see Figure 3). At finite temperatures the described effects are less dramatic, and the unit cell average spin grows continuously with the field from 0 at $H = 0$ (disordered state at finite T) to the saturated value $3\hbar/2$ as $H \leftarrow \mathfrak{R}$. The $H = 0$ results are corroborated by the calculation of the two-spin correlation function, which is related to the susceptibility through the fluctuation-dissipation theorem.

Actually, we have also found that $\varepsilon \sim \Upsilon \sim \exp[J/(k_B T)]/(k_B T)$, leading to the relation between the corresponding critical exponents $\nu = \rho = 2 - \gamma$, and from the behavior of the

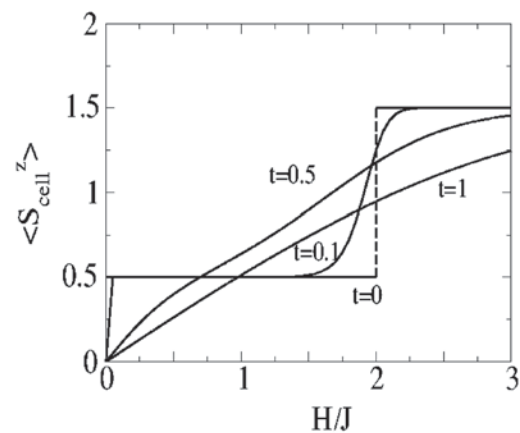


Figure 3. Average spin per unit cell, $\langle S_{cell}^z \rangle$, in units of \hbar , as function of the dimensionless magnetic field, H/J , and dimensionless temperature, $t = k_B T/J$, for the ferrimagnetic $S = 1/2 AB_2$ Ising chain.

correlation function at $T = 0$ and magnetization at $T = 0$ and $H \ll 0$ it follows that $\kappa = 1$ and $\zeta = \Re$. This set of exponents belongs to the same class of universality of decorated 1d ferromagnetic Ising systems.⁶⁸

Now, by considering Heisenberg spins in a classical context, in which quantum fluctuations are absent, the low- T and high- T limits of the $H = 0$ free energy and two-spin correlation functions have been calculated.⁴⁸ It is instructive to compare the $T \ll 0$ result obtained for the classical ferrimagnetic AB_2 Heisenberg chain,

$$\chi = \frac{2}{9} \frac{J}{(k_B T)^2} \left[1 - \frac{13}{4} \frac{k_B T}{J} + \dots \right] \quad (10)$$

with that of the classical ferromagnetic linear Heisenberg chain,⁶⁹

$$\chi = \frac{2}{3} \frac{J}{(k_B T)^2} \left[1 - \frac{1}{2} \frac{k_B T}{J} + \dots \right] \quad (11)$$

and that of Takahashi⁸ for the quantum ferromagnetic spin-1/2 linear Heisenberg chain,

$$\chi = \frac{2}{3} \frac{J}{(k_B T)^2} \left[1 - \frac{3\zeta(1/2)}{(2\pi)^{1/2}} \frac{(k_B T)^{1/2}}{J^{1/2}} + \frac{3\zeta^2(1/2)}{2\pi} \frac{k_B T}{J} + \dots \right] \quad (12)$$

where $\alpha(1/2)/(2\sigma)^{1/2} \approx -0.583$. At low- T Fisher's and Takahashi's leading terms coincide and are three times larger than that of the AB_2 chain, due to the unit-cell topology effect. Moreover, the second term in equation (12), absent in the classical models, is related to the fixing of the anomalous entropy and specific heat classical behaviors when quantum fluctuations are not present. We notice that this $\varepsilon \sim T^{-2}$ leading result as $T \ll 0$ has also been obtained for the semiclassical fixed point of the quantum $z = 2$ NL ϕ model, related to the quantum AB_2 Heisenberg chains (see above).

By taking quantum fluctuations into account, we also calculate⁶⁷ the three spin-wave modes of the quantum spin-1/2 AB_2 Heisenberg model using the Holstein-Primakov transformation and subsequent diagonalization via the Bogoliubov-Tyablikov method, namely, one non-dispersive optical, η_k^a , one dispersive optical, η_k^b , and one acoustical mode, η_k^c

$$\varepsilon_k^a = J + H,$$

$$\varepsilon_k^{b,c} = \frac{J}{2} \{ \pm 1 + [1 + 8 \sin^2(ka)]^{1/2} \} \mp H \quad (13)$$

Notice in the acoustical mode the presence of a quadratic ferromagnetic dispersion relation $\eta_k^c = 2J(ka)^2$, $ka \ll 1$, $H = 0$. From this result, corrections due to quantum

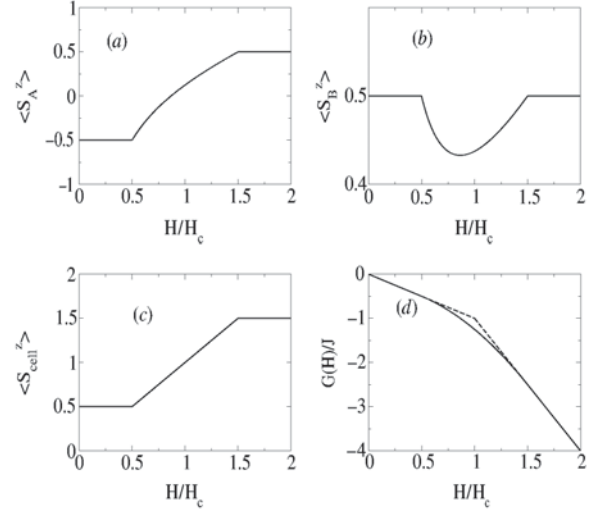


Figure 4. Average spin at sites A (a), sites B (b) and per unit cell (c), in units of \hbar , as function of the reduced field, H/H_c , for the quantum ferrimagnetic $S = 1/2$ AB_2 Heisenberg chain, with $H_c = 2J$. (d) The field dependence of the Gibbs free energy shows that the continuous solution (solid line) for the magnetization is the stable phase. The Ising-like solution is shown for comparison (dashed line).

fluctuations to the average values $\langle S_B^z \rangle = -\langle S_A^z \rangle = \hbar/2$ are derived, although the result of Lieb's theorem, $\langle S_{cell}^z \rangle = \hbar/2$, remains true. In a mean-field approach,^{48,67} we relate the quantum thermal spin averages at sites A and B to the respective Weiss molecular fields and find, in the simplest case in which they are assumed to be parallel to the z direction (Ising-like solution): $\langle S_B^z \rangle = \hbar/2$ for all $H \forall 0$, and $\langle S_A^z \rangle = -\hbar/2$ for $0 \leq H < H_c$, whereas $\langle S_A^z \rangle = \hbar/2$ for $H > H_c$. We notice that $H_c = 2J$ is the critical field below which the ferrimagnetic ordering is favoured, in agreement with the above result for the spin-1/2 AB_2 Ising model. Indeed, the unit cell spin reads $\langle S_{cell}^z \rangle = \hbar/2$ for $0 < H < H_c$, and $\langle S_{cell}^z \rangle = 3\hbar/2$ for $H > H_c$. On the other hand, in the case the x and y components are also considered, a quite interesting scenario emerges, with $\langle S_y^z \rangle = \pm \hbar/2$ for $0 \leq H < H_c/2$ and $\langle S_y^z \rangle = \hbar/2$ for $H > 3H_c/2$, where the plus (minus) sign refers to $\gamma = B$ (A) sites; for intermediate fields, $H_c/2 \leq H \leq 3H_c/2$ one has that $\langle S_A^z \rangle = -\hbar[3H_c/(4H) - H/H_c]/2$ and $\langle S_B^z \rangle = \hbar[3H_c/(8H) + H/(2H_c)]/2$. These results imply in the unit cell average spin $\hbar/2$ for $H < H_c/2$ with ferrimagnetism sustained, and the saturated $3\hbar/2$ value for $H > 3H_c/2$ as in the Ising-like solution. A linear increase with H arises for intermediate fields: $\langle S_{cell}^z \rangle = H/H_c$, for $H_c/2 < H < 3H_c/2$ (see Figure 4). In this regime the average spin at sites A continuously rotates seeking a full alignment with H , accompanied by a rotation of the spins at sites B , such that the transversal spin components at sites A and B always cancel out. To achieve this cancellation the spins at sites B rotate in the opposite direction up to a maximum polar angle $\tau = \sigma/6$ and then rotate back [see Figure 4(b)].

These results are corroborated by the analysis of the Gibbs free energy [Figure 4(d)].

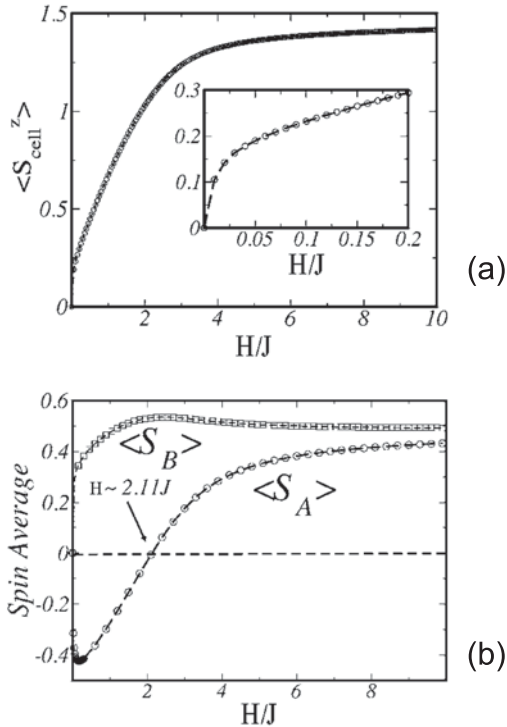


Figure 5. (a) Average spin per unit cell, $\langle S_{cell}^z \rangle$, and (b) spin averages at sites A (O) and B (□), in units of \hbar , as function of H/J , for $g = 0.05J$ and $T = 0.05J$, calculated for the quantum spherical $S = 1/2 AB_2$ model. Inset of (a): very-low-field regime.

At last, a spherical version of the quantum AB_2 spin Hamiltonian has also been studied.⁵¹ For this purpose, a chemical potential (μ) term is added to equation (2) in order to take care of the spherical constraint, $\text{tr}_{i\gamma} \langle S_{i\gamma}^z \rangle = N/4$, where N is the total number of sites. Quantum fluctuations are introduced, associated with a quantum coupling parameter g , through a kinetic energy term $(g/2) \text{tr}_{i\gamma} P_{i\gamma}^2$, in which $P_{i\gamma}$ are momentum operators canonically conjugated to each spin degree of freedom. By diagonalizing the Hamiltonian in a space of proper bosonic operators, we obtain two dispersive eigenmodes, also present in the linear AF spherical model, and a flatband induced by the AB_2 topology. At the only critical point, $g = T = H = 0$, the ferrimagnetic long-range order is present with $\langle S_B \rangle = -\langle S_A \rangle / \sqrt{2} = \hbar(3/16)^{1/2}$ and $\langle S_{cell}^z \rangle = \hbar(2^{1/2} - 1)(3/8)^{1/2}$. Interestingly, in the quantum AB_2 spherical case the average spin per unit cell is less than $\hbar/2$, in contrast with the result of Lieb's theorem for the AB_2 Hubbard model in the strong-coupling half-filled limit and the quantum AB_2 Heisenberg chain with AF couplings. Calculation of the correlation functions at $g = T = H = 0$ show that they are distance independent and finite, consistently with the ferrimagnetic order and the

spherical constraint. Outside this critical point, for any finite g , T or H , quantum and/or thermal fluctuations destroy the long-range order in the system, which in this case displays a finite maximum in the susceptibility. In this regime spins remain ferrimagnetically short-range ordered to some extent in the $\{g, T, H\}$ parameter space as a consequence of the AF interaction and the AB_2 topology. Indeed, we notice in Figure 5 that, although the field-induced unit cell average spin, $\langle S_{cell}^z \rangle$, displays quantum paramagnetic behavior for any finite g or T , the spins at sites A and B can display opposite orientations depending on the values of g , T and H . Therefore, for special regions of the parameter space $\{g, T, H\}$ spins at sites A points antiparallel with respect to those at sites B, thus giving rise to a rapid increase in the unit cell average spin for very low H and a field-induced short-range ferrimagnetism, which is destroyed for large g , T or H . In addition, to better characterize the approach to the $g = T = H = 0$ critical point, we have considered several paths. For $T \ll 0$ and $g = H = 0$ the susceptibility behaves as $\epsilon \sim T^{-2}$, as also found in several classical and quantum spherical and Heisenberg models (see above). On the other hand, for $H \ll 0$ and $g = T = 0$, we find $\epsilon \sim H^{-1}$, and for $g \ll 0$ and $T = H = 0$, $\epsilon \sim \exp(cg^{-1/2})$, where c is a constant, evidencing an essential singularity due to quantum fluctuations. In any path, the relation $\epsilon \sim \Upsilon^2$ is satisfied. We also mention that the known drawback of classical spherical models as $T \ll 0$ regarding the third law of thermodynamics (finite specific heat and diverging entropy) is fixed in the presence of quantum fluctuations, $g \in 0$.

3.2 Numerical results

The ferrimagnetic ordering can be probed through the magnetic structure factor:

$$S(q) = \frac{1}{N} \sum_{ij} e^{iq(x_i - x_j)} \langle \mathbf{S}_i \cdot \mathbf{S}_j \rangle \quad (14)$$

The condition for a long-range ferromagnetic ordering is that $S(0) \sim N$; while $S(\sigma) \sim N$ in a long-range antiferromagnetically ordered state. A ferrimagnetic long-range ordering fulfill these two conditions: $S(0) \sim N$ and $S(\sigma) \sim N$. This is the case for the AB_2 Hubbard and Heisenberg chains as exemplified in Figure 6 through the exact diagonalization (ED) of finite clusters. Due to the critical nature of both chains at low temperatures, the correlation length Υ and $\epsilon(q=0) = S(q=0)/(k_b T)$ satisfy power law behavior: $\Upsilon \sim T^{-\rho}$ and $\epsilon \sim T^{-\nu}$ as $T \ll 0$. Since $\Upsilon \sim N$ at $T = 0$, using scaling arguments and the results of Figure 6, we have $T^{-\nu} \sim T^{-\rho}/T$, i.e. $\nu - \rho = 1$, in agreement with the values $\nu = 2$ and $\rho = 1$ derived using renormalization group

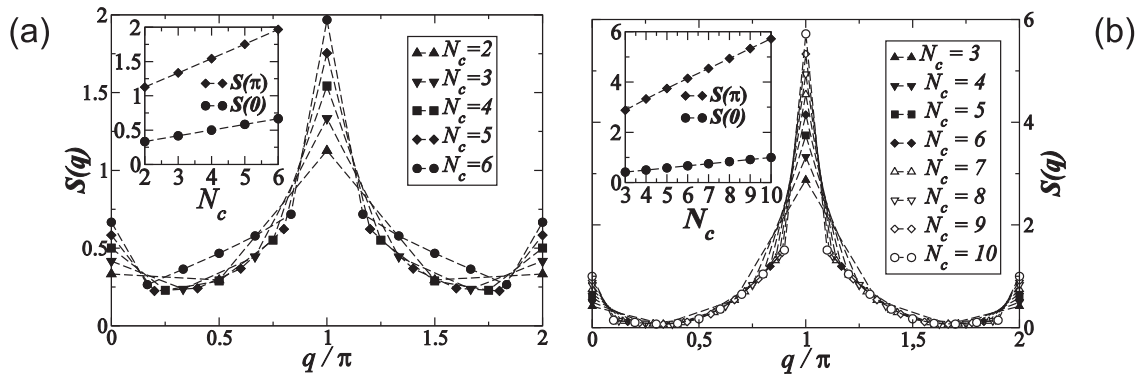


Figure 6. Magnetic structure factor $S(q)$ for (a) the AB_2 Hubbard chain with $U = 2t$ and (b) the AB_2 Heisenberg chain. The inset presents the size dependence of the ferromagnetic [$S(0)$] and antiferromagnetic [$S(\pi)$] peaks. Dashed lines are guides for the eye.

techniques. Furthermore, the ferrimagnetism of the model was also manifested through Hartree-Fock and quantum Monte Carlo methods.⁴³

Systems with a ferrimagnetic GS naturally have ferromagnetic (lowering the GS spin) and antiferromagnetic (rising the GS spin) magnons as their elementary magnetic excitations. The AB_2 chain have three spin wave branches:⁴⁶ an antiferromagnetic mode (AF mode), defined as $\pm E_{S^+}(q) = E(S^z = S_g + 1, q) - E_{GS}$; and two ferromagnetic ones (F1 and F2 modes), derived from $\pm E_{S^-}(q) = E(S^z = S_g - 1, q) - E_{GS}$, where E_{GS} is the GS energy and $E(S^z, q)$ are lowest energies in the sector $\{S^z, q\}$, with the lattice wave-vector $q = 2\sigma l/N_c$, where $l = 0, 1, \dots, N_c - 1$. These modes are depicted in Figure 7(a) for the Heisenberg model: the AF mode has a gap $\pm_{S^+} = 1.7591J$; the gapless F1 mode is the Goldstone mode, consistent with the symmetry broken phase of the chain; and the F2 mode has a gap $\pm_{S^-} = 1.0004J$. The gapped F2 branch is flat and is associated with the formation of a singlet state between the B sites in one cell, while the other cells have B sites in triplet states, as illustrated in Figure 7(b). The localized nature of the excitation is associated with the Hamiltonian invariance under the exchange of the B sites of any cell. This

symmetry implies that the many-body wave function has a definite parity under the exchange of the spatial variables associated with these sites. Since these dispersive modes preserve the local triplet bond, they are identical to those found in the spin-1/2 / spin-1 chain.⁷⁰ Surprisingly, linear spin wave theory (LSWT)⁶⁷ predicts that $\pm_{S^-} = 1$, very close to our estimated value: $\pm_{S^-} = 1.0004J$. Moreover, a good agreement is found for the gapless F1 branch in the long wave-length limit. However, both LSWT and mean field theory⁴⁸ predicts $\pm_{S^+} = 1$, deviating from our estimated exact diagonalization value: $\pm_{S^+} = 1.7591J$, which is in excellent agreement with numerical and analytical calculations for the spin-1/2 / spin-1 chain.⁷⁰ On the other hand, the interacting spin wave theory⁴⁷ derives a better result for \pm_{S^+} , but it implies in a higher shift for \pm_{S^-} (flat mode) not observed in our data of Figure 7(a).

On the other hand, the AF mode is relevant in the analysis of the response to an applied magnetic field H . The AF gap found above is responsible for a plateau in the curve of the magnetization per spin, $m(H) = \langle S^z \rangle / (N\hbar)$, as a function of H . In fact, it has been shown⁷¹ that if $\rho(s - m) = \text{integer}$, a plateau may appear in the magnetization curve of the Heisenberg model. In the last equation, s is

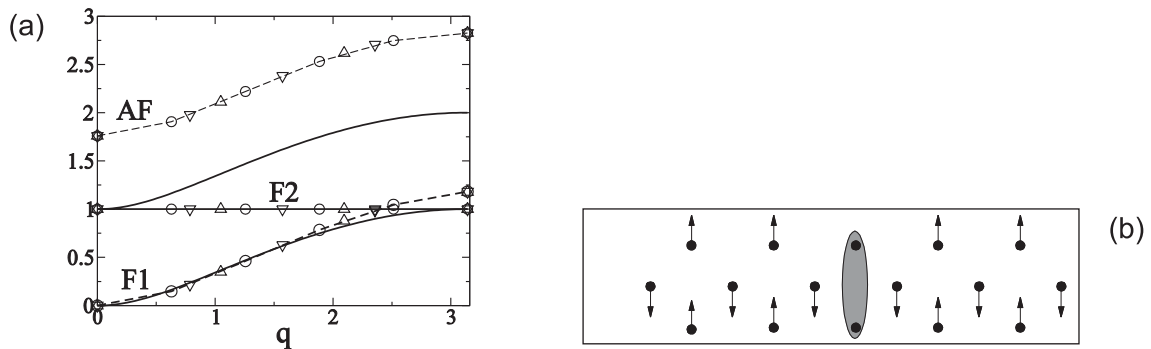


Figure 7. (a) Ferromagnetic (F) and antiferromagnetic (AF) spin wave modes of the Heisenberg AB_2 chain for $N_c = 10$ (circles), 8 (triangles down), 6 (triangles up). Solid lines are the linear spin wave results from reference 67; dashed lines are guides to the eye. (b) Illustration of the F2 mode: ellipse indicates a localized singlet state.

the site spin quantum number and ρ is the number of sites in one unit cell of the GS for a given value of H . The AB_2 Heisenberg chain has $s = 1/2$ and three sites per unit cell ($\rho = 3$); so, unless the system spontaneously breaks the translation invariance, we expect plateaus at $m = 1/6$ and $m = 1/2$. This is indeed what is observed in Figure 8. The plateau width at $m = 1/6$ is exactly given by \pm_{s+} , and is a measure of the stability of the ferrimagnetic phase. For higher fields, the magnetization increases in the expected way,⁷¹ as shown by the full line in Figure 8, before saturation at $m = 1/2$ for $H = 3J$. This field-dependent behavior contrasts with the linear one predicted by mean-field theory⁴⁸ shown in Figure 3. In fact, as predicted,⁷¹ the curve connecting the plateaus display square-root singularities, *i.e.*, $\sim |H-H_c|^{1/2}$, where H_c is the critical field at the edge of the plateaus. Exact diagonalization results⁴⁶ indicate that the antiferromagnetic spin gap and, consequently, the plateau at $m = 1/6$ exists for any finite value of U , with the plateau width (\pm_{s+}) nullifying as U^2 in the limit $U \leftarrow 0$.

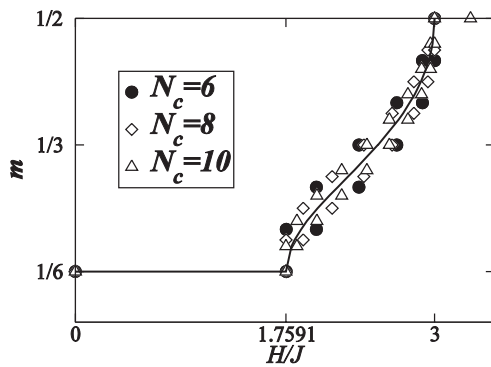


Figure 8. Magnetization as a function of the dimensionless applied magnetic field H/J for the AB_2 Heisenberg chain. The full line is a curve traced from the midpoints of the steps found in the finite size results, except at plateau regions.

Away from half-filling^{43,52} the AB_2 Hubbard model exhibits a rich phase diagram depending on the electronic density, $n \notin N_c/N$, or doping $\zeta (= 1 - n)$ from half-filling, and the Coulomb coupling U . The doped region was analyzed through Hartree-Fock⁴³, exact diagonalization^{43,52} and density matrix renormalization group (DMRG),⁵² which is the state-of-the-art method⁷² for the study of the GS properties of one-dimensional quantum lattice models. DMRG results suggest that in the underdoped region and for $U = 2t$, the ferrimagnetic phase sustains up to $\zeta \approx 0.02$, while for $0.02 < \zeta < 0.07$ hole itinerancy promotes incommensurate spin correlations (a spiral phase⁷³) with a ζ -dependent peak position in the magnetic structure factor, as shown in Figure 9(a) and (b). For $U = \mathfrak{R}$ and $\zeta = 0$ the GS total spin is degenerate, whereas for $0 < \zeta < 0.225$ hole itinerancy (Nagaoka mechanism^{74,75}) sets a fully polarized GS, as

shown in Figure 9(c). For higher doping, the system phase separates⁷⁶ into coexisting metallic and insulating phases for $\zeta_{ps}(U) < \zeta < 1/3$ [with $\zeta_{ps}(\mathfrak{R}) \approx 0.225$ and $\zeta_{ps}(2) \approx 0.07$]. In fact, the Hartree-Fock solution is unstable in this region and a Maxwell construction is needed.⁴³ The local parity symmetry is even (odd) in the insulating (metallic) phase. In Figure 10 we present spin correlation functions at $\zeta = 0.18$ ($\zeta = 0.28$) and $U = 2$ ($U = \mathfrak{R}$), calculated through DMRG (for these parameter values, the system is found in a phase separated state).

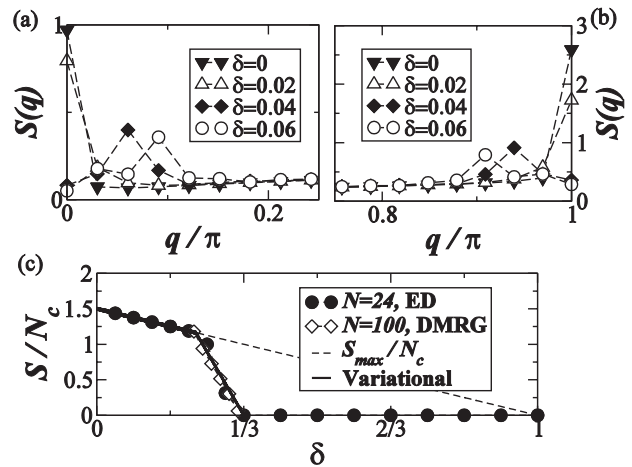


Figure 9. (a) and (b): Magnetic structure factor for $U = 2t$ and $N = 100$, using DMRG, in the underdoped region. (c) Total spin per cell S_g/N_c as function of ζ for $U = \mathfrak{R}$; the variational approach is described in reference 52.

In Figure 10(a) the correlation function between the spin at the extreme site of the phase with odd parities and the others spins, $\langle S_1 \cdot S_i \rangle$, evidences the spiral phase for $U = 2t$. For $U = \mathfrak{R}$ the local magnetization at sites A and B_1+B_2 shown in Figure 10(b) clearly displays the coexistence between the Nagaoka ferromagnetic phase and a paramagnetic one. Notice that, in the Nagaoka phase, the magnetization displays spatially modulated profiles due to hole itinerancy. Further, the local parity symmetries of the two coexisting phases are manifested in the correlation function between B spins at the same cell, $\langle S_{B_1} \cdot S_{B_2} \rangle$, shown in figures 10(c) and (d): in the phase with odd (even) parities cell triplet (singlet) states predominate. In Figure 10(e) we illustrate the phase separation for $U = \mathfrak{R}$. DMRG and exact diagonalization results⁵² indicate that the phase separation region ends precisely at $\zeta = 1/3$. For this doping the electronic system presents finite spin and charge gaps with very short ranged correlations and is well described by a short-ranged resonating-valence bond (RVB) state,⁷⁷ with the electrons correlated basically within a cell, as illustrated in Figure 10(f). A crossover region is observed for $1/3 \lesssim \zeta \lesssim 2/3$, while a Luttinger-liquid behavior⁷⁸ can be

explicitly characterized for $\zeta > 2/3$. Luttinger liquids are paramagnetic metals in one-dimension exhibiting power-law decay of the charge and spin correlation functions and the separation of the charge and spin excitation modes.

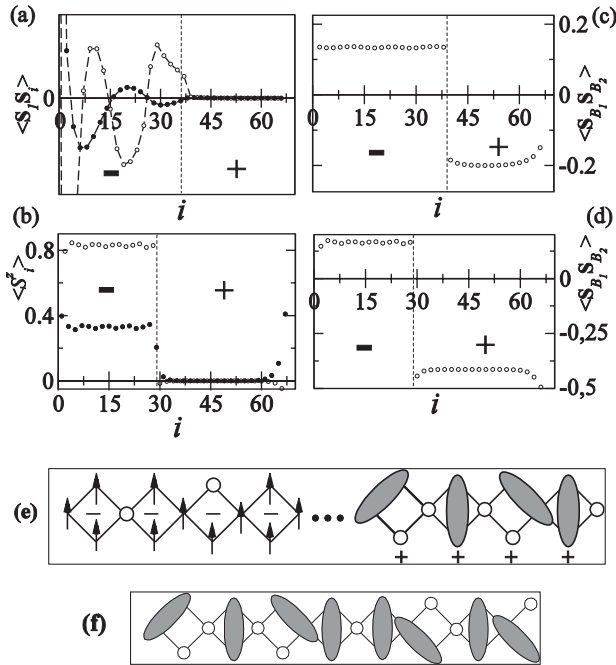


Figure 10. GS properties at $\zeta = 0.18$ ($U = 2t$) and $\zeta = 0.28$ ($U = \mathfrak{R}$) for $N = 100$ using DMRG. (a) Spin correlation function $\langle S_i \cdot S_j \rangle$ for $U = 2t$. (b) Expectation value of S_i^z for $U = \mathfrak{R}$ in the sector $S^z = S_g$. Spin correlation function $\langle S_{B_1} \cdot S_{B_2} \rangle$ for (c) $U = 2t$ and (d) $U = \mathfrak{R}$. Signal $-$ ($+$) indicates odd (even) local parity. Dashed lines are guides to the eye. Illustration of the GS for (e) $U = \mathfrak{R}$ in the phase-separated regime and (f) at $\zeta = 1/3$: singlet bonds are represented by ellipses and holes by circles.

In particular, the asymptotic behavior of the spin correlation function is given by

$$C_{LL}(l) \sim \frac{\cos(2k_F l) [\ln(l)]^{1/2}}{l^{1+K_\rho}} \quad (15)$$

where k_F is the Fermi wave vector and K_ρ is the model-dependent exponent. The predicted behavior in equation (15) fits very well the DMRG data at $\zeta = 88/106$ using $K_\rho = 0.89$ ($U = 2t$) and $K_\rho = 0.57$ ($U = \mathfrak{R}$), as shown in Figure 11. We remark that these values are close to 1 (noninteracting

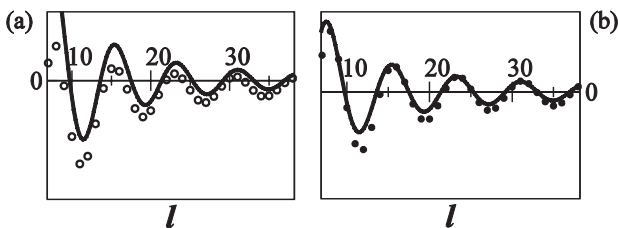


Figure 11. Spin correlation functions $C(l)$ for (a) $U = 2t$ and (b) $U = \mathfrak{R}$ at $\zeta = 88/106$ for $N = 106$ using DMRG: solid lines are fittings using equation (15).

fermions) and $1/2$ (noninteracting spinless fermions) for $U = 2t$ and $U = \mathfrak{R}$, respectively.

In addition, we mention that the commensurate doping $\zeta = 2/3$ is insulating, with a charge gap nullifying with U in a similar manner as the one of the Hubbard model in a linear chain at half-filling,⁷⁹ while the spin excitation is gapless.

4. Conclusions

In this contribution on the celebration of the 80th birthday anniversary of Prof. Ricardo Ferreira, we have presented a brief review of the main experimental and theoretical achievements on quasi-one-dimensional magnetic compounds, featuring those with AB_2 unit cell structure.

As reported, this has been an area of intense activity, particularly since the first experimental announcements in the mid 80's.¹⁻⁴ Nowadays several groups all over the world, involving chemists, physicists, and material scientists, are engaged in the characterization and description of properties of the already known materials, as well as doing great efforts towards the design and synthesis of new compounds, with novel properties suitable for technological applications.⁸⁰

From the fundamental point of view, these compounds have been used as a laboratory in which many theoretical concepts and predictions in the field of low-dimensional materials have been tested.

In conclusion, it seems clear that this interdisciplinary research area will remain an exciting and topical one for many years to come, offering new challenges both from the scientific and technological aspects.

Acknowledgments

We thank A. M. S. Macêdo, M. C. dos Santos, C. A. Macêdo and F. B. de Brito for collaboration in several stages of this research. Work supported by CNPq, CAPES, Finep and FACEPE (Brazilian agencies).



Maurício D. Coutinho-Filho is full Professor (Professor Titular) at the Physics Department of Universidade Federal de Pernambuco (UFPE). He received his PhD. degree in Physics in 1973 at Universidade de São Paulo. He also worked as a post-doc at Cornell University in 1974-1975,

and spent his sabbatical period during 1985-1986 at Harvard University. His research interests are statistical physics, field theory and numerical simulation in condensed matter: phase transitions, disordered systems, magnetism, metalinsulator transition, superfluidity, superconductivity and fluid dynamics, particularly flow in porous media.



Renê R. Montenegro-Filho is currently a post-doc at the Physics Department of UFPE, where he also received his PhD degree in Physics in 2006. His research interests are condensed matter physics, particularly strongly correlated

electron systems, with focus in magnetism and conductor-insulator transitions; and fluid dynamics, particularly flows in porous media.



Ernesto P. Raposo is Associate Professor (Professor Adjunto) at the Physics Department of UFPE, where he also received his PhD degree in Physics in 1996. He worked as a post-doc at Harvard University in 1996-1998. His research interests are statistical physics, field theory

and numerical simulation in condensed matter; disordered antiferromagnets; strongly correlated fermions: magnetism, metal-insulator transition and superconductivity; and statistical physics of the random search problem applied to ecology.



Carlindo Vitoriano is Associate Professor (Professor Adjunto) at the Campus of Garanhuns of the Universidade Federal Rural de Pernambuco (UFRPE). He received his PhD degree in Physics in 2000 at UFPE. He was also Associate

Professor at Universidade Salgado de Oliveira in the period 2000-2005. His research interests are statistical physics and condensed matter theory: critical phenomena and phase transitions; strongly correlated fermions: magnetism, metal-insulator transition and superconductivity.



Mário Henrique B. G. e Oliveira is Associate Professor (Professor Adjunto) at the Campus of Serra Talhada of the UFRPE. He received his PhD degree in Physics in 2006 at UFPE. His research interests are statistical physics and condensed

matter theory: critical phenomena and phase transitions; strongly correlated fermions.

References

1. Korshak, Y. V.; Medvedeva, T. V.; Ovchinnikov, A. A.; Spector, V. N.; *Nature* **1987**, 326, 370; Ovchinnikov, A. A.; Spector, V. N.; *Synth. Met.* **1988**, 27, B615 .
2. Takahashi, M.; Turek, P.; Nakazawa, Y.; Tamura, M.; Nozawa, K.; Shiomi, D.; Ishikawa, M.; Kinoshita, M.; *Phys. Rev. Lett.* **1991**, 67, 746; Tamura, M.; Nakazawa, Y.; Shiomi, D.; Nozawa, K.; Hosokoshi, Y.; Ishikawa, M.; Takahashi, M.; Kinoshita, M.; *Chem. Phys. Lett.* **1991**, 186, 401; Nakazawa, Y.; Tamura, M.; Shirakawa, N.; Shiomi, D.; Takahashi, M.; Kinoshita, M.; Ishikawa, M.; *Phys. Rev. B* **1992**, 46, 8906.
3. Kahn, O.; *Molecular Magnetism*, VCH: New York, 1993; Lahti, P. M. In *Magnetic Properties of Organic Materials*, Dekker: New York, 1999; See, also, Miller, J. S.; Epstein, A. J.; *Angew. Chem. Int. Ed. Engl.* **1994**, 33, 385.
4. Miller, J. S.; Krusic, P. J.; Epstein, A. J.; Reiff, W. M.; Zhang, J. H.; *Mol. Cryst. Liq. Cryst.* **1985**, 120, 27; Chittipeddi, S.; Cromack, K. R.; Miller, J. S.; Epstein, A. J.; *Phys. Rev. Lett.* **1987**, 58, 2695; Miller, J. S.; Epstein, A. J.; *Angew. Chem. Int. Ed. Engl.* **1994**, 33, 385; Miller, J. S.; Epstein, A. J.; *Chem. Commun.* **1998**, 13, 1319.
5. Silvestre, J.; Hoffmann, R.; *Inorg. Chem.* **1985**, 24, 4108.
6. Nishide, H.; *Adv. Mater.* **1995**, 7, 937.
7. Ivanov, C. I.; Olbrich, G.; Barentzen, H.; Polansky, O. E.; *Phys. Rev. B* **1987**, 36, 8712 .
8. Yamada, M.; Takahashi, M.; *J. Phys. Soc. Japan* **1985**, 54, 2808; Takahashi, M.; *Phys. Rev. Lett.* **1997**, 58, 168; Schlottmann, P.; *Phys. Rev. Lett.* **1985**, 54, 2131; Schlottmann, P.; *Phys. Rev. B* **1986**, 33, 4880.
9. Yoshizawa, K.; Tanaka, K.; Yamabe, T.; Yamauchi, J.; *J. Chem. Phys.* **1992**, 96, 5516; Baumgarten, M.; Müllen, K.; Tyutyulkov, N.; Madjarova, G.; *Chem. Phys.* **1993**, 169, 81; Sariciftci, N. S.; Heeger, A. J.; Cao, Y.; *Phys. Rev. B* **1994**, 49, 5988.
10. Kohlman, R. S.; Joo, J.; Wang, Y. Z.; Pouget, J. P.; Kaneko, H.; Ishiguro, T.; Epstein, A. J.; *Phys. Rev. Lett.* **1995**, 74, 773; Yoshioka, K.; Masubuchi, S.; Kazama, S.; Mizoguchi, K.; Kume, K.; Sakamoto, H.; Kachi, N.; *Synth. Met.* **1997**, 84, 695. For related compounds, see: Lu, H. S. M.; Berson, J. A.; *J. Am. Chem. Soc.* **1997**, 119, 1428.
11. Wynn, C. M.; Girtu, M. A.; Miller, J. S.; Epstein, A. J.; *Phys. Rev. B* **1997**, 56, 14050; Wynn, C. M.; Girtu, M. A.; Zhang, J.; Miller, J. S.; Epstein, A. J.; *Phys. Rev. B* **1998**, 58, 8508.
12. Caneschi, A.; Gatteschi, D.; Renard, J. -P.; Rey, P.; Sessoli, R.; *Inorg. Chem.* **1989**, 28, 1976; Caneschi, A.; Gatteschi, D.; Renard, J. -P.; Rey, P.; Sessoli, R.; *Inorg. Chem.* **1989**, 28, 2940; Caneschi, A.; Gatteschi, D.; Renard, J. -P.; Rey, P.; Sessoli, R.; *J. Am. Chem. Soc.* **1989**, 111, 785.

13. Drillon, M.; Coronado, E.; Belaiche, M.; Carlin, R. L.; *J. Appl. Phys.* **1988**, *63*, 3551.
14. Abu-Youssef, M. A. M.; Escuer, A.; Goher, M. A. S.; Mautner, F. A.; Rei, G. J.; Vicente, R.; *Angew. Chem. Int. Ed.* **2000**, *39*, 1624.
15. Coronado, E.; Drillon, M.; Fuertes, A.; Beltran, D.; Mosset, A.; Galy, J.; *J. Am. Chem. Soc.* **1986**, *108*, 900.
16. Coronado, E.; Drillon, M.; Nugteren, P. R.; de Jongh, L. J.; Beltran, D.; *J. Am. Chem. Soc.* **1988**, *110*, 3907.
17. Escuer, A.; Vicente, R.; Fallah, M. S. E.; Goher, M. A. S.; Mautner, F. A.; *Inorg. Chem.* **1998**, *37*, 4466.
18. Abu-Youssef, M. A. M.; Drillon, M.; Escuer, A.; Goher, M. A. S.; Mautner, F. A.; Vicente, R.; *Inorg. Chem.* **2000**, *39*, 5022.
19. Cano, J.; Journaux, Y.; Goher, M. A. S.; Abu-Youssef, M. A. M.; Mautner, F. A.; Reiß, G. J.; Escuer, A.; Vicente, R.; *New J. Chem.* **2005**, *29*, 306.
20. Reis, M. S.; Moreira dos Santos, A.; Amaral, V. S.; Brando, P.; Rocha, J.; *Phys. Rev. B* **2006**, *73*, 214415.
21. Kahn, O.; Pei, Y.; Verdaguer, M.; Renard, J.-P.; Sletten, J.; *J. Am. Chem. Soc.* **1988**, *110*, 782.
22. Van Koningsbruggen, P. J.; Kahn, O.; Nakatani, K.; Pei, Y.; Renard, J. -P.; *Inorg. Chem.* **1990**, *29*, 3325.
23. Verdaguer, M.; Julve, M.; Michalowicz, A.; Kahn, O.; *Inorg. Chem.* **1983**, *22*, 2624; Pei, Y.; Verdaguer, M.; Kahn, O.; Sletten, J.; Renard, J. -P.; *Inorg. Chem.* **1987**, *26*, 138; Van Koningsbruggen, P. J.; Khan, O.; Nakatani, K.; Pei, Y.; Renard, J. P.; Drillon, M.; Legoll, P.; *Inorg. Chem.* **1990**, *29*, 3325.
24. Pati, S. K.; Ramasesha, S.; Sen, D.; *Phys. Rev. B* **1997**, *55*, 8894; Yamamoto, S.; Brehmer, S.; Mikeska, H. -J.; *Phys. Rev. B* **1998**, *57*, 13610; Ivanov, N. B.; *Phys. Rev. B* **2000**, *62*, 3271. Yamamoto, S.; *Phys. Rev. B* **2004**, *69*, 064426; and references therein.
25. Kahn, O.; Bakalbassis, E.; Mathonire, C.; Hagiwara, M.; Katsumata, K.; Ouahab, L.; *Inorg. Chem.* **1997**, *36*, 1530.
26. Clérac, R.; Miyasaka, H.; Yamashita, M.; Coulon, C.; *J. Am. Chem. Soc.* **2002**, *124*, 12837.
27. Iwamura, H.; Inoue, K.; Koga, N.; *New J. Chem.* **1998**, *22*, 201.
28. Ovchinnikov, A. S.; Bostrem, I. G.; Sinitsyn, V. E.; Baranov, N. V.; Inoue, K.; *J. Phys.: Condens. Matter* **2001**, *13*, 5221.
29. Ovchinnikov, A. S.; Bostrem, I. G.; Sinitsyn, V. E.; Boyarchenkov, A. S.; Baranov, N. V.; Inoue, K.; *J. Phys.: Condens. Matter* **2002**, *14*, 8067.
30. Wynn, C. M.; Girtu, M. A.; Miller, J. S.; Epstein, A. J.; *Phys. Rev. B* **1997**, *56*, 315; Wynn, C. M.; Girtu, M. A.; Sugiura, K.-I.; Brandon, E. J.; Manson, J. L.; Miller, J. S.; Epstein, A. J.; *Synth. Met.* **1997**, *85*, 1695; Wynn, C. M.; Girtu, M. A.; Brinckerhoff, W. B.; Sugiura, K.-I.; Miller, J. S.; Epstein, A. J.; *Chem. Mater.* **1997**, *9*, 2156; Brandon, E. J.; Arif, A. M.; Burkhart, B. M.; Miller, J. S.; *Inorg. Chem.* **1998**, *37*, 2792; Brandon, E. J.; Rittenberg, D. K.; Arif, A. M.; Miller, J. S.; *Inorg. Chem.* **1998**, *37*, 3376.
31. Fegy, K.; Luneau, D.; Belorizky, E.; Novac, M.; Tholence, J. -L.; Paulsen, C.; Ohm, T.; Rey, P.; *Inorg. Chem.* **1998**, *37*, 4524.
32. Seiden, J.; *J. Phys. Lett.* **1983**, *44*, 947.
33. Anderson, J. B.; Kostiner, E.; Ruzsala, F. A.; *J. Solid State Chem.* **1981**, *39*, 29.
34. Drillon, M.; Belaiche, M.; Legoll, P.; Aride, J.; Boukhari, A.; Moqine, A.; *J. Magn. Magn. Mater.* **1993**, *128*, 83.
35. Belik, A. A.; Matsuo, A.; Azuma, M.; Kindo, K.; Takano, M.; *J. Solid State Chem.* **2005**, *178*, 709.
36. Matsuda, M.; Kakurai, K.; Belik, A. A.; Azuma, M.; Takano, M.; Fujita, M.; *Phys. Rev. B* **2005**, *71*, 144411.
37. Boukhari, A.; Moqine, A.; Flandrois, S.; *Mater. Res. Bull.* **1986**, *21*, 395.
38. Effenberger, H.; *J. Solid State Chem.* **1999**, *142*, 6.
39. Kikuchi, H.; Fujii, Y.; Chiba, M.; Mitsudo, S.; Idehara, T.; Tonegawa, T.; Okamoto, K.; Sakai, T.; Kuwai, T.; Ohta, H.; *Phys. Rev. Lett.* **2005**, *94*, 227201.
40. Okamoto, K.; Tonegawa, T.; Kaburagi, M.; *J. Phys. Condens. Matter.* **2003**, *15*, 5979; Fu, H. H.; Yao, K. L.; Liu, Z. L.; *Phys. Rev. B* **2006**, *73*, 104454; Fu, H. H.; Yao, K. L.; Liu, Z. L.; *Solid State Commun.* **2006**, *139*, 289; Gu, B.; Su, G.; *Phys. Rev. B* **2007**, *75*, 174437.
41. Hosokoshi, Y.; Katoh, K.; Nakazawa, Y.; Nakano, H.; Inoue, K.; *J. Am. Chem. Soc.* **2001**, *123*, 7921; Yao, K. L.; Liu, Q. M.; Liu, Z. L.; *Phys. Rev. B* **2004**, *70*, 224430; Yao, K. L.; Fu, H. H.; Liu, Z. L.; *Solid State Commun.* **2005**, *135*, 197. See also the AB_2 quasi-1d compound $Cu_3(TeO_3)_2Br_2$; Uematsu, D.; Sato, M.; *J. Phys. Soc. Jpn.* **2007**, *76*, 084712.
42. Lieb, E. H.; *Phys. Rev. Lett.* **1989**, *62*, 1201. See, also, Tian, G.-S.; Lin, T.-H.; *Phys. Rev. B* **1996**, *53*, 8196; for this special AB_2 topology.
43. Macêdo, A. M. S.; dos Santos, M. C.; Coutinho-Filho, M. D.; Macedo, C. A.; *Phys. Rev. Lett.* **1995**, *74*, 1851.
44. de Melo, C. P.; Azevedo, S. A. F.; *Phys. Rev. B* **1996**, *53*, 16258.
45. Duan, Y. F.; Yao, K. L.; *Phys. Rev. B* **2001**, *63*, 134434. Wang, W. Z.; Hu, B.; Yao, K. L.; *Phys. Rev. B* **2002**, *66*, 085101.
46. Montenegro-Filho, R. R. ; Coutinho-Filho, M. D.; *Physica A* **2005**, *357*, 173.
47. Nakanishi, T.; Yamamoto, S.; *Phys. Rev. B* **2002**, *65*, 214418. Recent results for spin waves in the double-chain ferrimagnets $A_3Cu_3(PO_4)_4$ (A=Ca, Sr, Pb) can be found in: Yamamoto, S.; Ohara, J.; *Phys. Rev. B* **2007**, *76*, 014409.
48. Vitoriano, C.; Coutinho-Filho, M. D.; Raposo, E. P.; *J. Phys. A* **2002**, *35*, 9049. For Ising-Heisenberg and Ising diamond chains, see: Canová, L.; Strecka, J.; Jascur, M.; *J. Phys. Condens. Matter* **2006**, *18*, 4967; Fu, H. H.; Yao, K. L.; Liu, Z. L.; *J. Magn. Magn. Mater.* **2006**, *305*, 253.
49. Alcaraz, F. C.; Malvezzi, A. L.; *J. Phys. A* **1997**, *30*, 767.
50. Raposo, E. P.; Coutinho-Filho, M. D.; *Phys. Rev. B* **1999**, *59*, 14384; *Phys. Rev. Lett.* **1997**, *78*, 4853.

51. Oliveira, M. H.; Coutinho-Filho, M. D.; Raposo, E. P.; *Phys. Rev. B* **2005**, *72*, 214420. For a review on classical and quantum spherical spin models, see: Brankov, J. G.; Danchev, D. M.; Tonchev, N. S.; *Theory of Critical Phenomena in Finite-Size Systems*, World Scientific: Singapore, 2000, and references therein.
52. Montenegro-Filho, R. R.; Coutinho-Filho, M. D.; *Phys. Rev. B* **2006**, *74*, 125117.
53. Sierra, G.; Martín-Delgado, M. A.; White, S. R.; Scalapino, D. J.; Dukelsky, J.; *Phys. Rev. B* **1999**, *59*, 7973.
54. Watanabe, Y.; Miyashita, S.; *J. Phys. Soc. Jpn.* **1999**, *68*, 3086.
55. Martín-Delgado, M. A.; Rodriguez-Laguna, J.; Sierra, G.; *Phys. Rev. B* **2005**, *72*, 104435.
56. Raposo, E. P.; Coutinho-Filho, M. D.; *Mod. Phys. Lett. B* **1995**, *9*, 817.
57. Lieb, E. H.; Mattis, D. C.; *J. Math. Phys.* **1962**, *3*, 749. See, also, Tian, G.-S.; *J. Phys. A: Math. Gen.* **1994**, *27*, 2305.
58. Fradkin, E.; *Field Theories of Condensed Matter Systems*, Addison-Wesley: Redwood City, 1991; chap. 5; Tselik, A. M.; *Quantum Field Theory in Condensed Matter Physics*, Cambridge University Press: Cambridge, 1996; chaps. 7-10.
59. Haldane, F. D. M.; *Phys. Rev. Lett.* **1983**, *50*, 1153; Affleck, I.; *Nucl. Phys. B* **1985**, *257*, 397.
60. Klein, D. J.; Nelin, C. J.; Alexander, S.; Matsen, F. A.; *J. Chem. Phys.* **1982**, *77*, 3101.
61. Tyutyulkov, N.; Schuster, P.; Polansky, O.; *Theor. Chim. Acta* **1983**, *63*, 291; Tyutyulkov, N.; Karabunarliev, S.; Müllen, K.; Baumgarten, M.; *Synth. Met.* **1992**, *52*, 71; Tyutyulkov, N.; Dietz, F.; Müllen, K.; Baumgarten, M.; Karabunarliev, S.; *Theor. Chim. Acta* **1993**, *86*, 353; Madjarova, G.; Baumgarten, M.; Müllen, K.; Tyutyulkov, N.; *Macromol. Theory Simul.* **1994**, *3*, 803; Beust, R.; Tyutyulkov, N.; Rabinovitzb, M.; Dietz, F.; *Chem. Phys.* **1999**, *240*, 141; and references therein.
62. Nelson, D. R.; Pelcovits, R. A.; *Phys. Rev. B* **1977**, *16*, 2191.
63. Chakravarty, S.; Halperin, B. I.; Nelson, D. R.; *Phys. Rev. Lett.* **1988**, *60*, 1057; *Phys. Rev. B* **1989**, *39*, 2344; Chakravarty, S.; *Phys. Rev. Lett.* **1996**, *77*, 4446; Sachdev, S.; *Phys. Rev. B* **1997**, *55*, 142.
64. Fisher, M. P. A.; Weichman, P. B.; Grinstein, G.; Fisher, D. S.; *Phys. Rev. B* **1989**, *40*, 546.
65. Continentino, M. A.; *Phys. Rep.* **1994**, *239*, 179; Continentino, M. A.; *Quantum Scaling in Many-Body Systems*, World Scientific: Singapore, 2001.
66. Yang, K.; *Phys. Rev. Lett.* **2004**, *93*, 066401.
67. Vitoriano, C.; de Brito, F. B.; Raposo, E. P.; Coutinho-Filho, M. D.; *Mol. Cryst. Liq. Cryst.* **2002**, *374*, 185.
68. Nelson, D. R.; Fisher, M. E.; *Ann. Phys.* **1975**, *91*, 226; Maris, H. J.; Kadanoff, L. P.; *Am. J. Phys.* **1978**, *46*, 652.
69. Fisher, M. E.; *Am. J. Phys.* **1964**, *32*, 343. See, also, Bonner, J. C.; Fisher, M. E.; *Phys. Rev.* **1964**, *135*, A640.
70. Yamamoto, S.; Brehmer, S.; Mikeska, H. -J.; *Phys. Rev. B* **1998**, *57*, 13610; Ivanov, N. B.; *Phys. Rev. B* **2000**, *62*, 3271. Yamamoto, S.; *Phys. Rev. B* **2004**, *69*, 064426.
71. Oshikawa, M.; Yamanaka, M.; Affleck, I.; *Phys. Rev. Lett.* **1997**, *78*, 1984. Connection with magnon Bose-Einstein condensation can be found in: Affleck, I.; *Phys. Rev. B* **1991**, *43*, 3215; Sorensen, E. S.; Affleck, I.; *Phys. Rev. Lett.* **1993**, *71*, 1633. See also Tselick, A. M.; *Phys. Rev. B* **1990**, *42*, 10499. For recent results on the field and temperature behavior of the magnetization of gapped Haldane spin-1 chains, see: Moeda, Y.; Hotta, C.; Oshikawa, M.; *Phys. Rev. Lett.* **2007**, *99*, 057205.
72. White, S. R.; *Phys. Rev. B* **1993**, *48*, 10345; Schollwöck, U.; *Rev. Mod. Phys.* **2005**, *77*, 259.
73. Schulz, H. J.; *Phys. Rev. Lett.* **1990**, *64*, 1445; Andersen, M. B.; Hedegard, P.; *Phys. Rev. Lett.* **2005**, *95*, 037002.
74. Nagaoka, Y.; *Phys. Rev.* **1966**, *147*, 392.
75. Tasaki, H.; *Prog. Theor. Phys.* **1998**, *99*, 489; and references therein, including those describing the occurrence of flat band or nearly flat band - saturated ferromagnetism at finite U .
76. See, e. g., Emery, V. J.; Kivelson, S. A.; Lin, H. Q.; *Phys. Rev. Lett.* **1990**, *64*, 475; Dagotto, E.; *Science* **2005**, *309*, 257.
77. Rokhsar, D. S.; Kivelson, S. A.; *Phys. Rev. Lett.* **1988**, *61*, 2376; see, also, Anderson, P. W.; *The Theory of Superconductivity in the High- T_c Cuprates*, Princeton University Press: Princeton, 1997, and references therein.
78. Haldane, F. D. M.; *J. Phys. C* **1981**, *14*, 2585; Voit, J.; *Rep. Prog. Phys.* **1995**, *58*, 977; Giamarchi, T.; *Quantum Physics in One Dimension*, Oxford University, Press: New York, 2004.
79. Lieb, E. H.; Wu, F. Y.; *Phys. Rev. Lett.* **1968**, *20*, 1445; Lieb, E. H.; Wu, F. Y.; *Physica A* **2003**, *321*, 1.
80. See, e. g., Morin, B. G.; Hahn, C.; Miller, J. S.; Epstein, A. J.; *J. Appl. Phys.* **1994**, *75*, 5782; Epstein, A. J.; *MRS Bulletin* **2003**, *28*, 492.

Received: September 12, 2007

Published on the web: February 22, 2008